

# Adsorption mechanism of sodium polysulfide clusters on selenium-doped $\text{Ti}_2\text{CO}_2$ MXenes for application in sodium-sulfur batteries

To Trong Mai<sup>1</sup>, Nguyen Truong Long<sup>1</sup>, Duong Trong Nhan<sup>1</sup>, Nguyen Thi Bao Trang<sup>1,2</sup>, Pham Vu Nhat<sup>1</sup>, Duy Khanh Nguyen<sup>3,4</sup>, Minh Triet Dang<sup>1,\*</sup>



Use your smartphone to scan this QR code and download this article

## ABSTRACT

Room-temperature sodium-sulfur batteries demonstrate significant potential for future energy storage applications. However, several challenges, including the shuttle effect and low conductivity, hinder their practical implementation. The shuttle effect not only results in energy loss but also adversely impacts the electrochemical performance of the batteries. The migration of polysulfides can lead to a gradual reduction in battery capacity as well as the cycling performance. Furthermore, low conductivity may inhibit charge transfer, slow reaction kinetics, and diminish overall battery efficiency. To address these challenges, utilizing two-dimensional (2D) MXenes as electrode anchoring materials presents a promising solution. This approach can effectively mitigate the shuttle effect and enhance the electronic conductivity of sodium-sulfur batteries. This study aims to investigate the effects of doping selenide atoms into 2D MXenes through first-principles methods to improve sodium-sulfur batteries' stability and electronic properties. The introduction of selenide atoms into the termination layer is intended to capture sodium polysulfide clusters. Our findings indicate that doping  $\text{Ti}_2\text{CO}_2$  MXenes with selenide atoms enhances the interaction between the Se-4p and S-3p orbitals, improving their ability to adsorb  $\text{Na}_2\text{S}$  and  $\text{Na}_2\text{S}_2$  clusters compared to the pristine systems. We provide a detailed discussion of the bonding mechanisms between the  $\text{Na}_2\text{S}_x$  clusters and the selenide-doped MXenes. Additionally, we highlight the differences in adsorption mechanisms between low-sulfur content clusters ( $\text{Na}_2\text{S}$ ,  $\text{Na}_2\text{S}_2$ , and  $\text{Na}_2\text{S}_4$ ) and high-sulfur content clusters ( $\text{Na}_2\text{S}_6$  and  $\text{Na}_2\text{S}_8$ ), with a focus on charge transfers and electronic properties. The unique structure of MXenes allows them to interact effectively with polysulfides, which can help suppress the shuttle effect, preventing polysulfide migration and reducing energy loss. Moreover, the enhanced conductivity provided by MXenes facilitates improved charge transfer, leading to superior overall performance in sodium-sulfur batteries. Our results emphasize the crucial role of selenide atoms in 2D MXene electrode materials, as they enhance the adsorption mechanisms of sodium polysulfides for applications in sodium-sulfur rechargeable batteries.

**Key words:** Sodium-sulfur batteries, MXenes, Selenium doping, Anchoring materials, Density functional theory

<sup>1</sup>Department of Physics Education, Can Tho University, 3/2 Street, Ninh Kieu District, Can Tho, Vietnam

<sup>2</sup>FPT University, 600 Nguyen Van Cu, Ninh Kieu District, Can Tho, Vietnam

<sup>3</sup>Laboratory for Computational Physics, Institute for Computational Science and Artificial Intelligence

<sup>4</sup>Faculty of Mechanical - Electrical and Computer Engineering, School of Technology, Van Lang University, Ho Chi Minh, Viet Nam

## Correspondence

**Minh Triet Dang**, Department of Physics Education, Can Tho University, 3/2 Street, Ninh Kieu District, Can Tho, Vietnam

Email: dmtriet@ctu.edu.vn

## History

- Received: 04-11-2024
- Revised: 25-12-2024
- Accepted: 10-10-2025
- Published Online: xx-xx-2026

## DOI :



## INTRODUCTION

Currently, the development of portable electronic devices has driven our demand for rechargeable batteries; thus, lithium-ion batteries are emerging as the preferred choice due to their high energy density, lightweight design, and long lifespan<sup>1</sup>. However, the depletion of lithium sources and the threshold for the energy density of lithium-ion batteries have made the push to our research for alternative ion batteries<sup>2,3</sup>. Recent reviews provide an overview of the current state of non-lithium rechargeable batteries based on  $\text{Na}^+$ ,  $\text{K}^+$ ,  $\text{Ca}^+$ , and  $\text{Mg}^+$ <sup>4,5</sup>. These alternative ion batteries are promoted as the next generation of high-density, environmentally friendly, and low-cost batteries. One of the most promising cathode materials

is sodium, especially with the sodium-sulfur (Na-S) batteries. Na-S batteries have garnered significant attention recently due to their low-cost components and considerable energy density<sup>6</sup>. Various studies evaluate the performance of Na-S batteries<sup>7-11</sup> and predict the transition from lithium-sulfur and lithium-oxygen batteries to sodium-sulfur batteries<sup>7</sup>. However, the practical implementation of sodium-sulfur battery technology still faces several challenges. One recognized obstacle is the shuttle effect, which impedes sulfur ions from reaching their neutral state and participating in the charging and discharging process. This effect is due to the dissolution of higher-order sodium polysulfides in common electrolyte solvents during cycling<sup>8-11</sup> and causes self-discharge

**Cite this article :** Mai TT, Long NT, Nhan DT, Bao Trang NT, Vu Nhat P, Nguyen DK, Dang MT. **Adsorption mechanism of sodium polysulfide clusters on selenium-doped  $\text{Ti}_2\text{CO}_2$  MXenes for application in sodium-sulfur batteries.** Sci. Tech. Dev. J. – Engineering and Technology 2026; x(x):xxxx-xxxx.

**Copyright**

© VNUHCM Press. This is an open-access article distributed under the terms of the Creative Commons Attribution 4.0 International license.



and rapid decay of active materials. Additionally, the poor electrical conductivity of the sulfur cathode poses another problem for the Na-S battery. To prevent the shuttle effect, a common approach is to use sulfur-host anchoring materials to capture sodium polysulfides and bind these molecules at the cathode surface<sup>12,13</sup>. Thus, anchoring materials must strongly bind to the sodium polysulfide clusters, exceeding the binding of Na-S molecules with electrolytes.

Two-dimensional MXene material, a group of 2D transition metal carbides, nitrides, and carbonitrides, has shown great promise in Li-S and Na-S batteries due to its excellent electrical conductivity, high surface area, and mechanical robustness<sup>14,15</sup>. Anchoring materials based on MXene have shown potential as they can efficiently trap polysulfides on the surface, provide a conducive framework for sulfur species, and enhance electronic conductivity<sup>16-18</sup>. Research on MXene's application in sodium-sulfur batteries is still ongoing, but initial studies have shown promising results in improving their electrochemical performance. This study provides a detailed first-principles analysis of Se-doped  $\text{Ti}_2\text{CO}_2$  MXene, exploring its structural, electronic, and adsorption properties for potential use in sodium-sulfur batteries. The substitution of oxygen with selenium on the termination layer transforms  $\text{Ti}_2\text{CO}_2$  from a small band-gap semiconductor into a metallic conductor, enhancing its electronic properties. The adsorption energies of various  $\text{Na}_2\text{S}_x$  clusters ( $x = 1, 2, 4, 6, 8$ ) on the Se-doped MXene are thoroughly examined, revealing a particularly strong interaction with low-sulfur content clusters. This strong binding is crucial for mitigating the shuttle effect, a key challenge in Na-S batteries. Bader charge analysis supports these findings by showing significant charge transfer, especially with lower-sulfur clusters, further improving electrochemical interactions. Our results highlight Se-doped  $\text{Ti}_2\text{CO}_2$  MXene as a promising anchoring material, offering deep insights into its chemical interactions with sodium polysulfides and paving the way for advanced Na-S battery technology.

## COMPUTATIONAL METHODS

We employ density functional theory (DFT) via the Quantum Espresso package<sup>19</sup> to study the adsorption of  $\text{Na}_2\text{S}_x$  clusters ( $x = 1, 2, 4, 6, 8$ ) on a modified 2D layer  $\text{Ti}_2\text{CO}_2$  with Se doping on the terminal surface, so-called  $\text{Ti}_2\text{CO}_2(\text{Se})$ . Our DFT calculations use the exchange-correlation in the generalized gradient approximation (GGA) by the PBE functional<sup>20</sup>, obtained from the standard solid-state pseudo-potentials library<sup>21</sup>, and the van der

Waals interactions (vdW-DF3)<sup>22,23</sup> is included. Our Monkhorst-Pack  $\Gamma$ -centered k-grids are  $4 \times 4 \times 1$  and  $8 \times 8 \times 1$  for Brillouin zone sampling in structural optimization and electronic structure calculations, respectively. The energy cut-off is set at 60 Ry, the convergence threshold for the self-consistent field calculations is at  $10^{-8}$  eV/Å, and the optimal force condition is  $10^{-4}$  eV. Calculated parameters of energy cut-off and k-grid are based on ref.<sup>24,25</sup>. Our convergence thresholds for self-consistent field and force condition are default values provided by the Quantum Espresso package.

Firstly, we optimized a 2D pristine  $\text{Ti}_2\text{CO}_2$  structure with the supercell of  $3 \times 3 \times 1$  and based on the space group  $P\bar{3}m1$ ,  $Z = 164$ , and lattice parameters reported in ref.<sup>24</sup> to obtain the 2D structure of  $\text{Ti}_2\text{CO}_2$  MXene. Our model contains a vacuum space of 20 Å along the z-direction to eliminate the effect of periodic images, commonly employed in modeling 2D materials. To examine the effect of Se doping on the termination surface of 2D  $\text{Ti}_2\text{CO}_2$ , we modified the  $3 \times 3 \times 1$  supercell by replacing an O atom with a Se atom and then optimizing the model to find the most favorable energetic configuration. An analysis was conducted on several doped sites for the selenium (Se) doping atom to identify the site with the lowest energy, indicating the most favorable energetic configuration for Se. The optimized model corresponding to this site will further investigate sodium polysulfide adsorption.

To determine the optimized adsorption configuration of  $\text{Na}_2\text{S}_x$  clusters on the  $\text{Ti}_2\text{CO}_2(\text{Se})$ , various possible adsorption sites of the MXene and different rotations of  $\text{Na}_2\text{S}_x$  clusters are examined to find the lowest energy configuration. We set the initial height of the  $\text{Na}_2\text{S}_x$  clusters on the top layer of MXenes at 2.5 Å. The adsorption energy ( $E_{ads}$ ) of each cluster on MXenes is calculated as:

$$E_{ads} = E_{cluster-MXene} - E_{cluster} - E_{MXene} \quad (1)$$

where  $E_{cluster-MXene}$  and  $E_{MXene}$  denote the total energies of the MXene with and without  $\text{Na}_2\text{S}_x$  clusters, respectively, and  $E_{cluster}$  is the energy of the optimized  $\text{Na}_2\text{S}_x$  clusters. For each  $\text{Na}_2\text{S}_x$  adsorbate, we only reported the best configurations for the adsorbed  $\text{Na}_2\text{S}_x$  on MXene and performed further analyses. Bader charge calculation based on Henkelman's algorithm<sup>26</sup> via Critic2<sup>27</sup> is used to indicate charge transfer between the adsorbed sodium polysulfide and the MXenes.

## RESULTS AND DISCUSSION

### Structure of Se doped on the surface of Ti<sub>2</sub>CO<sub>2</sub> MXene

We first elucidate the optimized structure of 2D Ti<sub>2</sub>CO<sub>2</sub> and then determine the possible sites for Se doping on the termination surface via DFT optimization to obtain the most favored equilibrium configuration in energy. We found that the doped Se atom will be located at the same symmetrical site of surface O atoms but at a higher height than the termination O-layer. These optimized structures of 2D Ti<sub>2</sub>CO<sub>2</sub> without and with Se doping on the termination O-layer of MXene are illustrated in Figure 1. Our optimized lattice constants, Ti-C bonding length, and Ti-O bonding length of 2D Ti<sub>2</sub>CO<sub>2</sub> (space group  $\bar{P}3m1$  ( $Z = 164$ )) are 2.98 Å, 2.16 Å, and 1.95 Å, respectively. These results agree well with previous reports<sup>24,25,28,29</sup>. These MXenes consist of hierarchical Ti and C layers sandwiched between two terminated layers of the oxygen functional groups. For the Se doping site on the termination surface, we substituted one O atom with Se atom and optimized the doping structure, as shown in Figure 1b. The substitution of the Se atom at one site of 2D Ti<sub>2</sub>CO<sub>2</sub> on the termination layer induces a slight deformation to the geometry structure, as the height of Se atom on c-direction emerges on top of O-plane. The defect formation energy of the doped Se on 2D Ti<sub>2</sub>CO<sub>2</sub> is calculated using equation (2).

$$E^f [Se\_doped] = E_{tot} [Ti_2CO_2 (Se)] - E_{tot} [Ti_2CO_2] + n_i \mu_O - n_i \mu_{Se}$$

where  $E_{tot} [Ti_2CO_2 (Se)]$  and  $E_{tot} [Ti_2CO_2]$  are the total energies of the bare supercell Ti<sub>2</sub>CO<sub>2</sub> and Ti<sub>2</sub>CO<sub>2</sub>(Se), respectively. The defect is created due to the substituted  $n_i$  atoms and  $\mu_O, \mu_{Se}$  are chemical potentials of O and Se atoms, which are calculated as energies per atom from O<sub>2</sub> molecules and S<sub>8</sub> ring isolated in a cubic cell. Hence, the defect formation energy value is reported at 3.26 eV for the doped Se atom replacing the O atom on 2D Ti<sub>2</sub>CO<sub>2</sub>. This result is comparable to the defect formation energy at 2.47 eV of doping S atom on 2D Ti<sub>3</sub>C<sub>2</sub>O<sub>2</sub><sup>30</sup>.

### Adsorption of Na<sub>2</sub>S<sub>x</sub> clusters on Ti<sub>2</sub>CO<sub>2</sub>(Se) MXene

We now investigate the adsorption mechanism of Na<sub>2</sub>S<sub>x</sub> clusters on the Se-doped Ti<sub>2</sub>CO<sub>2</sub> MXene. The optimized adsorption sites of the Na<sub>2</sub>S<sub>x</sub> clusters on the terminal oxygen layers of Ti<sub>2</sub>CO<sub>2</sub>(Se) MXenes

are presented in Figure 2. Several possible configurations were examined, and we present here the preferred configuration with the lowest energies. The overall alignments of Na<sub>2</sub>S<sub>x</sub> and S<sub>8</sub> clusters upon adsorption on the surface of Ti<sub>2</sub>CO<sub>2</sub>(Se) are similar to the adsorption of MXene and other 2D materials<sup>8,24</sup>. Figure 2 demonstrates that the S<sub>8</sub> cluster is weakly adsorbed parallel to the MXene, while low-S content Na<sub>2</sub>S<sub>x</sub> clusters ( $x = 1,2,4$ ) tend to have two Na atoms aligned horizontally toward the termination layer. On the other hand, high-S content clusters of Na<sub>2</sub>S<sub>6</sub> and Na<sub>2</sub>S<sub>8</sub> are usually adsorbed with Na atoms aligned vertically to the termination layer. Interestingly, the Na<sub>2</sub>S<sub>x</sub> and S<sub>8</sub> clusters are driven toward the doped Se sites. Figure 2 points out that the doping Se atom on the termination layer attracts one pair of S and Na atoms of low-S content Na<sub>2</sub>S<sub>x</sub> clusters (Na<sub>2</sub>S, Na<sub>2</sub>S<sub>2</sub>, Na<sub>2</sub>S<sub>4</sub>) into the adjacent vicinity of the Se doping site. Otherwise, only one Na atom is attracted to the doping Se atom high-S content clusters of Na<sub>2</sub>S<sub>6</sub> and Na<sub>2</sub>S<sub>8</sub>, and the S-ring structure is likely to stay on top of the termination layer near the doping site. The S<sub>8</sub> ring is aligned vertically and symmetrically on top of the doped Se atom.

To assess the capability of anchoring Na-S cluster on Ti<sub>2</sub>CO<sub>2</sub>(Se) for Na-S battery, we calculated the adsorption energies of Na<sub>2</sub>S<sub>x</sub> clusters on Ti<sub>2</sub>CO<sub>2</sub>(Se) in Figure 3. Negative adsorption energies indicate that the Na<sub>2</sub>S<sub>x</sub> clusters can be efficiently anchored on the MXene surface. For inhibition of the shuttle effect, the adsorption energies of Na<sub>2</sub>S<sub>x</sub> clusters on Ti<sub>2</sub>CO<sub>2</sub>(Se) should be higher than the binding energy of Na<sub>2</sub>S<sub>x</sub> with common electrolyte solvents such as DOL and DME, commonly reported at below 1 eV in Refs.<sup>8,24,31,32</sup>. Therefore, we aim to anchor materials with good adsorption energies to bind the Na<sub>2</sub>S<sub>x</sub> clusters with the battery anode. Remarkably, all clusters exhibit considerable negative adsorption energies, varying between -1.01 eV (S<sub>8</sub>) and -3.44 eV (Na<sub>2</sub>S). Hence, our calculated adsorption energies for Ti<sub>2</sub>CO<sub>2</sub> and Ti<sub>2</sub>CO<sub>2</sub>(Se) are significantly higher than the binding energy of Na<sub>2</sub>S<sub>x</sub> with common electrolyte solvents. Therefore, this indicates that Ti<sub>2</sub>CO<sub>2</sub> and Ti<sub>2</sub>CO<sub>2</sub>(Se) are promising anchoring materials for sodium sulfur ion batteries. Our results of Ti<sub>2</sub>CO<sub>2</sub> are comparable to the adsorption energies from -0.948 eV to -3.113 eV of Na<sub>2</sub>S<sub>x</sub> clusters on bare Ti<sub>2</sub>CO<sub>2</sub> in ref.<sup>24</sup>. Notably, our adsorption energies for Ti<sub>2</sub>CO<sub>2</sub>(Se) are increased in most of Na-S clusters, indicating that it is a promising method to enhance the anchoring ability. We found that the adsorption energies of S<sub>8</sub> and high-S content Na<sub>2</sub>S<sub>x</sub> clusters are much weaker than those of low-S content

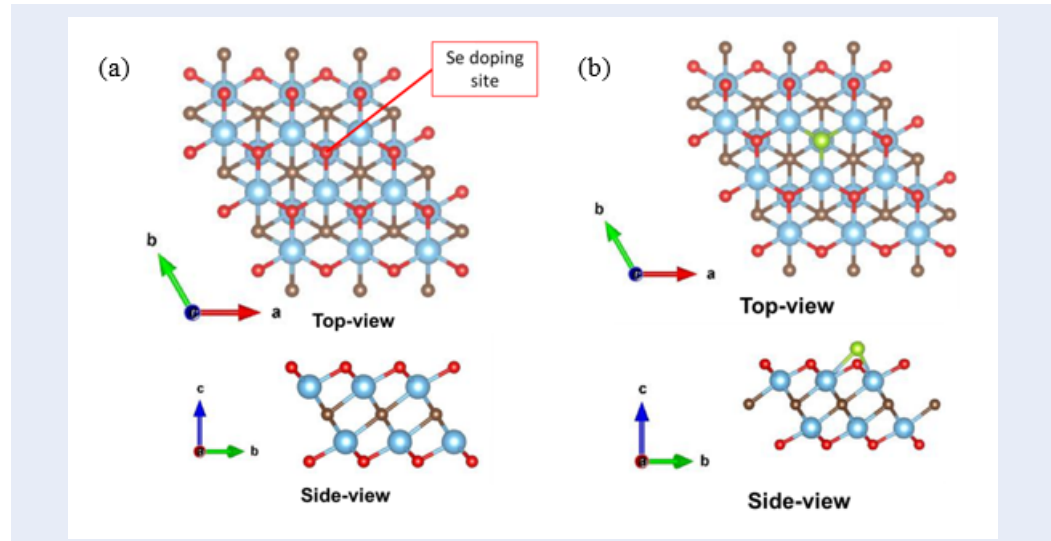


**Figure 1:** (a) Top- and side-view of the optimized geometrical structures of  $\text{Ti}_2\text{CO}_2$  and optimized doped site on the terminal layer for Se atom. (b) Top- and side-view for the most favored energetically configuration of Se doping on the termination surface of  $\text{Ti}_2\text{CO}_2$ . The light blue, red, brown, and green balls illustrate Ti, O, C, and Se atoms, respectively.

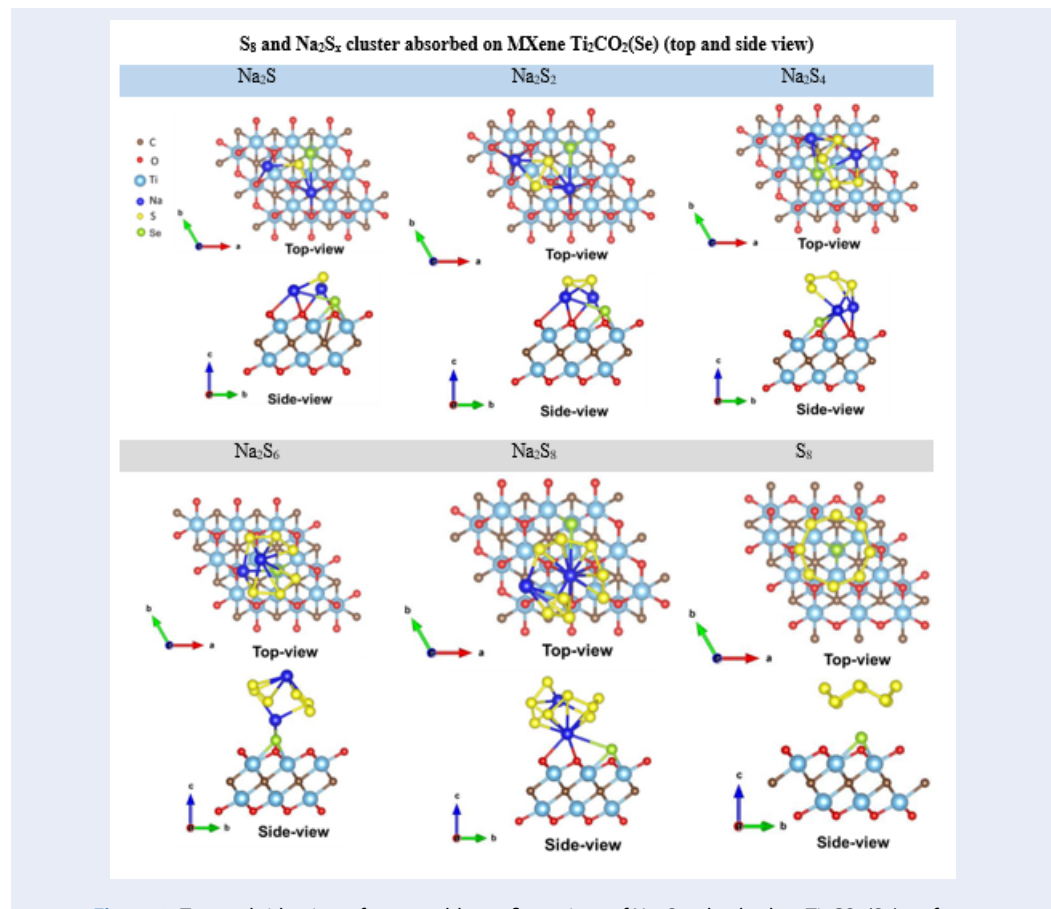


**Figure 2:** Top- and side-view of most stable configurations of  $\text{Na}_2\text{S}_x$  adsorbed on  $\text{Ti}_2\text{CO}_2(\text{Se})$  surface.

$\text{Na}_2\text{S}_x$  clusters. Note that  $\text{Na}_2\text{S}$  clusters have the highest adsorption energies with  $\text{Ti}_2\text{CO}_2(\text{Se})$  concerning other  $\text{Na}_2\text{S}_2$  clusters upon adsorption on other 2D materials<sup>10,24</sup>. Currently, pure carbon-based anchoring materials such as graphite, graphene, or graphene oxide are utilized in Na-S batteries<sup>8,10,33</sup>. However, the weak adsorption of these 2D layers with Na-S clusters ( $E_{ads}$  is from 0.5 to 1.3 eV) is considered an insufficient solution to deal with the shuttle effect. Hence, the  $\text{Ti}_2\text{CO}_2$  and Se-doping  $\text{Ti}_2\text{CO}_2$  proved to have advanced capacity compared to current carbon-based anchoring materials. Our results also indicate that the doped Se atom binds Na-S clusters better than bare  $\text{Ti}_2\text{CO}_2$  and provides a promising method to capture Na-S clusters better.

To obtain insight into the high binding energies, we examine the out-of-plane z-height of Se atom, height of Na atom on top of O-plane, and the bond length of Se-Na, Na-O, Se-S, and S-O of the adsorbed systems in Figure 4. As shown in Figure 4a, the doped Se atom is located at 0.85 Å on top of the termination O-layer and this height of Se atom is increase upon absorption of  $\text{Na}_2\text{S}_x$  clusters. The adsorbed  $\text{Na}_2\text{S}$  on  $\text{Ti}_2\text{CO}_2(\text{Se})$ , which exhibits the highest adsorption energy, also possesses the highest height of Se. The z-position of Se on top of the termination layer tends to be lower in high S-content clusters. On the opposite, the height of the Na atom on top of the termination layer in adsorbed high-S content is higher than the other system, as shown in Figure 4b. This means that the presence of the Se atom is attracted to low S-content  $\text{Na}_2\text{S}_x$  clusters. Figure 4 c indicates that the Se-Na bonds are longer than the Na-O bonds. Hence, the formation of Na-O bonding is one of the primary interactions, whereas Se-Na bonding contributes as a secondary interaction. However, while the S-O bonding fluctuates around 3.40 Å, the Se-O bonding of  $\text{Na}_2\text{S}$  and  $\text{Na}_2\text{S}_2$  is shorter than the other Se-O bondings. Upon adsorption, S atoms in these two clusters are strongly bound to the Se atom on the MXene surface, thus enhancing the adsorption energy.

### Electronic and charge transfer upon adsorption of $\text{Na}_2\text{S}_x$ clusters on MXene

We now explore the effect of doped Se on the termination layer of  $\text{Ti}_2\text{CO}_2$  on the electronic properties and charge transfer. Theoretically, the density-of-state (DOS) in electronic properties determines the electronic conductivity, and analysis of the partial density-of-state (PDOS) upon adsorption provides detailed information for the change in electronic conductivity and chemical hybridization of molecular

orbitals<sup>34</sup>. Partial density-of-state (PDOS) of  $\text{Ti}_2\text{CO}_2$  without and with doping of the Se atom on the termination layer is shown in Figure 5. From the PDOS of pristine  $\text{Ti}_2\text{CO}_2$ , it expresses as a small band-gap semiconductor with  $E_{gap} = 0.25$  eV, comparable to the calculated value of 0.2 - 0.3 eV from other DFT calculations<sup>29,33,35,36</sup>. Its PDOS features that the valence states just below the Fermi level are mainly contributed by C 2p, Ti 3d, and O 2p orbitals, consistently to other works<sup>25,29,33,36</sup>. Besides, the further peak of valence states contain most by C 2p and in secondary, Ti 3d, and O 2p orbitals. At the energy higher than the Fermi level, conducting states of bare  $\text{Ti}_2\text{CO}_2$  present a dominated peak of Ti 3d orbitals and a lesser contribution of O 2p orbitals. For the Se-doping  $\text{Ti}_2\text{CO}_2(\text{Se})$ , contributions from Se 4p are located below the Fermi level to -3.5 eV. By substituting one O atom with a Se atom, a peak of O 2p orbitals at -1.2 eV is replaced by the Se 4p orbitals, and the band gap is significantly reduced to the metal characteristic. Hence, the se-doping on  $\text{Ti}_2\text{CO}_2$  induces an electronic transition to close the semiconducting gap, which is preferred for the sulfur host of sodium-sulfur batteries<sup>30,34</sup>. The electron-rich p-state in the doped Se atom is closer to the Fermi level, which enhances the desired electronic conductivity and high carrier mobility for our anchoring materials. It agrees with another study of S-doped on  $\text{Ti}_3\text{C}_2\text{O}_2$  MXene, indicating that highly polarized electron-rich S doping donates its electrons to improve the electronic conductivity of the MXenes<sup>30</sup>.

Furthermore, we evaluate the electronic properties and calculate charge transfer upon adsorption of  $\text{Na}_2\text{S}_x$  clusters on  $\text{Ti}_2\text{CO}_2(\text{Se})$ . The PDOS of the adsorbed  $\text{Na}_2\text{S}_x$  (where  $x = 1, 2, 4, 6, 8$ ) systems are shown in Figure 6. Upon adsorption, the metallic characteristics of  $\text{Ti}_2\text{CO}_2(\text{Se})$  MXene are preserved; thus, good conductivity is maintained. Compared to the PDOS of  $\text{Ti}_2\text{CO}_2(\text{Se})$ , weak interaction of the surface layer with  $\text{S}_8$  does not represent any significant change in the electronic states of the MXene. In contrast, during the adsorption of  $\text{Na}_2\text{S}$ , the proportion of Se 4p states below the Fermi level is the most modified. It is due to the strong interaction of Se 4p states overlapping with S 3p states in the range of 0 eV - 3 eV in agreement with the stronger Se-S bond shown in Figure 4d. For other PDOS of  $\text{Ti}_2\text{CO}_2(\text{Se})$  adsorbed  $\text{Na}_2\text{S}_x$  clusters, there are several pronounced peaks appear on the low energies below and above Fermi level belong to the S 3p states. We found that p-states of the doping Se atom hybridize with p-states of S atoms, causing strong chemical bonding for  $\text{Na}_2\text{S}$ ,  $\text{Na}_2\text{S}_2$ , and  $\text{Na}_2\text{S}_4$ . This explained the change in Se height in Figure 4a and short

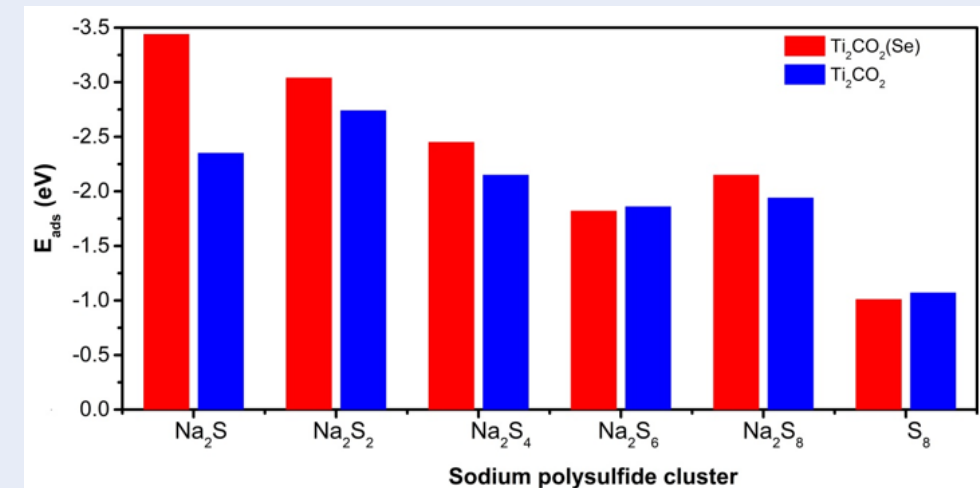


**Figure 3:** Adsorption energies  $E_{ads}$  calculated for  $\text{Na}_2\text{S}_x$  clusters adsorbed on  $\text{Ti}_2\text{CO}_2(\text{Se})$  compared to bare 2D  $\text{Ti}_2\text{CO}_2$  MXene

S-Se bonds for smaller adsorbed  $\text{Na}_2\text{S}_x$  clusters in Figure 4c.

To analyze the complex mechanism of cluster adsorption on the surface, we calculate Bader charges to quantify electron transfers during adsorption. In the Na-S adsorption case, strong chemical interaction is often due to a considerable charge transfer, which can be revealed by differential charge analysis. This technique is commonly employed in several studies of Na-S and Li-S adsorption<sup>34,37</sup>. Figure 7 provides an overview of the Bader charges of the different adsorbed clusters. For instance,  $\text{S}_8$  clusters only transfer a negligible number of charges (0.08 e) to the MXene, which confirms the weak interaction of the  $\text{S}_8$  cluster. In addition, the Se atom carries a slight charge transfer with the  $\text{S}_8$  cluster. In contrast with insignificant charge transfer for  $\text{S}_8$ , our adsorptions of  $\text{Na}_2\text{S}$ ,  $\text{Na}_2\text{S}_2$ , and  $\text{Na}_2\text{S}_4$  exhibit considerable charge transfers of 0.98-1.04 e for 2D  $\text{Ti}_2\text{CO}_2(\text{Se})$ . For high S-content clusters of  $\text{Na}_2\text{S}_6$  and  $\text{Na}_2\text{S}_8$ , the charge transfer decreased to 0.43 e and 0.37 e for 2D  $\text{Ti}_2\text{CO}_2(\text{Se})$ , respectively. Significant charge transfers between Na-S clusters with the surface atoms in Figure 7 also display that our adsorptions in  $\text{Na}_2\text{S}$ ,  $\text{Na}_2\text{S}_2$ , and  $\text{Na}_2\text{S}_4$  are due to strong chemical interaction, agreed with results in<sup>37</sup>. Therefore, doping the Se atom on 2D  $\text{Ti}_2\text{CO}_2$  leads to more charge transfer, which renders enhanced adsorption energies and more charge redistribution from Na-S clusters to the MXene, especially for the adsorption of the small clusters. Both of them are beneficial for the electrochemical performance of Na-S batteries.

## CONCLUSION

In this study, we systematically study modified surfaces via Se doping on  $\text{Ti}_2\text{CO}_2$  MXene for anchoring the sodium polysulfides in application in Na-S batteries. Using first-principle calculations, we examine the optimized 2D structure of Se-doped  $\text{Ti}_2\text{CO}_2$  and its electronic structure. Upon adsorption,  $\text{Ti}_2\text{CO}_2(\text{Se})$  exhibits a considerably higher binding capability towards  $\text{Na}_2\text{S}_x$  clusters than common electrolyte solvents, especially for the  $\text{Na}_2\text{S}$  cluster. We demonstrate that a doped Se atom could improve the adsorption ability of 2D  $\text{Ti}_2\text{CO}_2$  to suppress the shuttle effect better. We also analyzed the bonding between  $\text{Na}_2\text{S}_x$  and the doped Se and O atoms on the termination surface.  $\text{Ti}_2\text{CO}_2(\text{Se})$  shows a reduced band gap to the metallic state by incorporating the Se atom on the termination surface. The adsorption of  $\text{Na}_2\text{S}$  clusters to the  $\text{Ti}_2\text{CO}_2(\text{Se})$  expresses strong interaction between Se 4p and S 3p states. Our Bader charge difference signifies that the charge transfers from  $\text{Na}_2\text{S}_x$  clusters of low S-content ( $\text{Na}_2\text{S}$ ,  $\text{Na}_2\text{S}_2$ , and  $\text{Na}_2\text{S}_4$ ) to  $\text{Ti}_2\text{CO}_2(\text{Se})$  are higher than from the high S-content ( $\text{Na}_2\text{S}_6$  and  $\text{Na}_2\text{S}_8$ ). More charge transfer and strong chemical interaction of Na-S cluster with the Se-doped  $\text{Ti}_2\text{CO}_2$  surface are beneficial for the electrochemical performance of Na-S batteries. Thus, these results demonstrate the significant contribution of doped Se atoms on  $\text{Ti}_2\text{CO}_2$  MXene electrodes as anchoring materials for application in sodium-sulfide batteries.

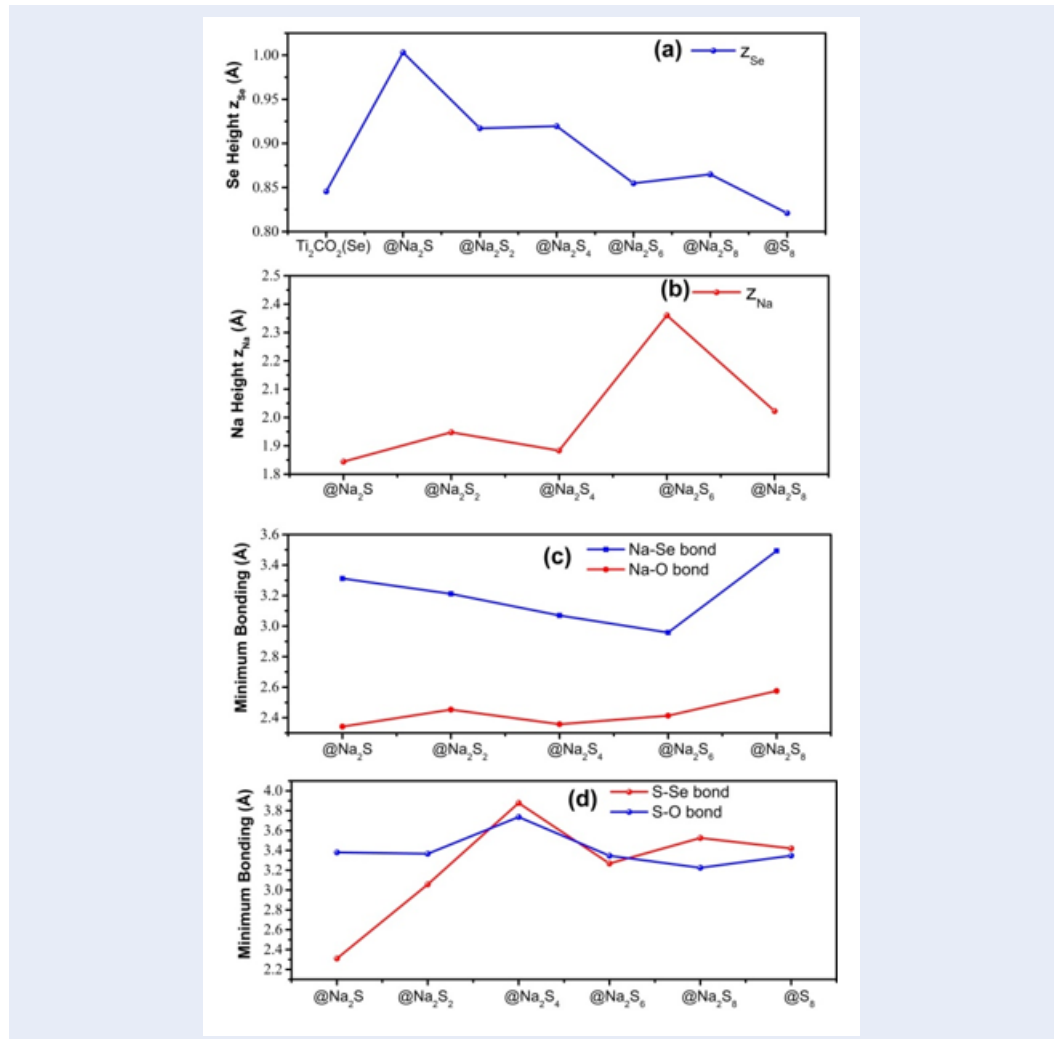


**Figure 4:** (a-b) The height distances on c-direction  $z_{\text{Se}}$  and  $z_{\text{Na}}$  compared to the termination O-layer (c-d) the minimum bond length of Se-Na, Na-O, Se-S, and S-O pairs.

## ABBREVIATIONS LIST

2D: Two Dimensional  
 Se: Selenide  
 S: Sulfur  
 Na: Sodium  
 MXenes: Family of Two Dimensional Carbides and Nitrides of Transition Metals  
 DFT: Density Functional Theory  
 Na-S: Sodium-Sulfur  
 $\text{Na}_2\text{S}_x$ : Sodium-Sulfur clusters ( $\text{Na}_2\text{S}$ ,  $\text{Na}_2\text{S}_2$ ,  $\text{Na}_2\text{S}_4$ ,  $\text{Na}_2\text{S}_6$ ,  $\text{Na}_2\text{S}_8$ )  
 $\text{S}_8$ : cluster of Sulfur molecule  
 $\text{Ti}_2\text{CO}_2(\text{Se})$ : Se-doped on O-terminated layer of  $\text{Ti}_2\text{CO}_2$  MXene  
 $E_{\text{ads}}$ : Adsorption Energy

$E_{\text{cluster-MXene}}$ : Total Energies of the MXene with adsorbed  $\text{Na}_2\text{S}_x$  clusters calculated by DFT  
 $E_{\text{MXene}}$ : Total Energies of the bare MXene calculated by DFT  
 $E_{\text{cluster}}$ : Energy of the Optimized  $\text{Na}_2\text{S}_x$  Clusters  
 $\bar{P}3m1$ : Spacegroup name of  $Z = 164$  from Hermann-Mauguin notation  
 GGA: Generalized Gradient Approximation  
 PBE: Perdew-Burke-Ernzerhof functional  
 vdW-DF3: van der Waals interactions functional  
 $E^f(\text{Se_doped})$ : defect formation energy of the doped Se on 2D  $\text{Ti}_2\text{CO}_2$   
 $E_{\text{tot}}[\text{Ti}_2\text{CO}_2(\text{Se})]$ : total energies of the bare supercell  $\text{Ti}_2\text{CO}_2$   
 $E_{\text{tot}}(\text{Ti}_2\text{CO}_2)$ : total energies of the bare supercell  $\text{Ti}_2\text{CO}_2$  and  $\text{Ti}_2\text{CO}_2(\text{Se})$ ,

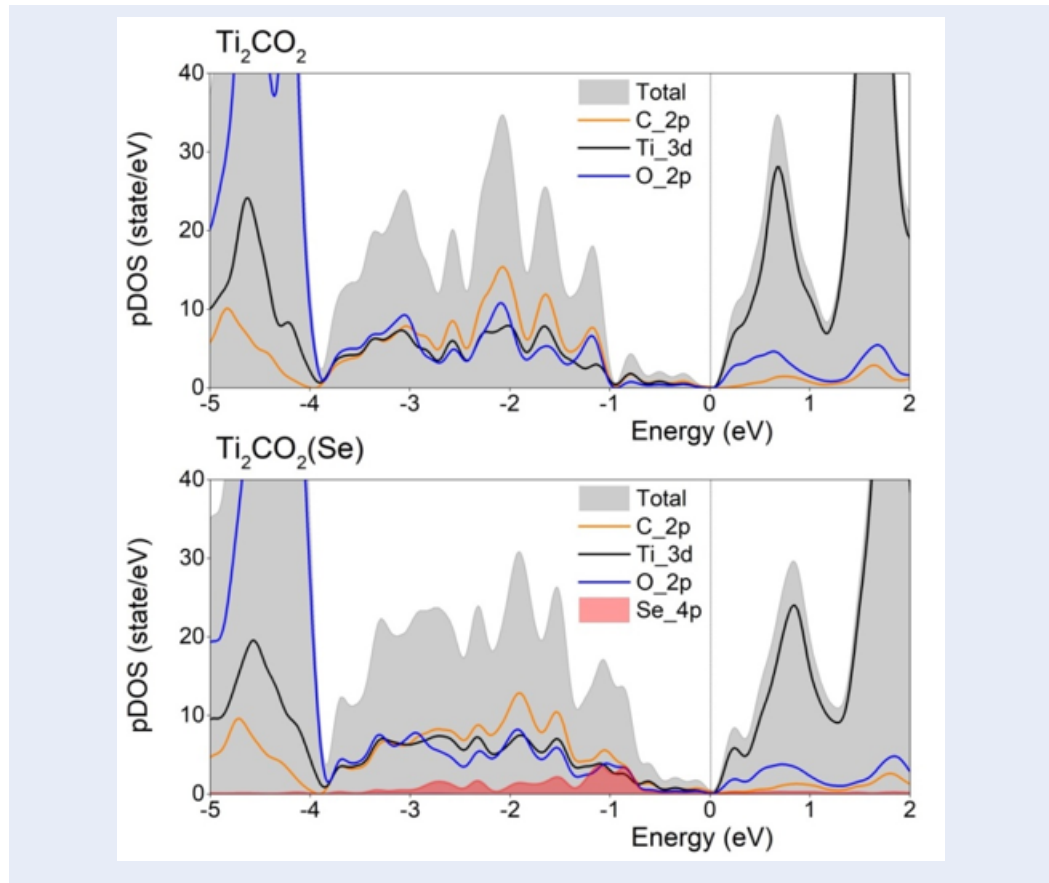


**Figure 5:** Projected density of states (PDOS) of bare  $\text{Ti}_2\text{CO}_2$  and doped  $\text{Ti}_2\text{CO}_2(\text{Se})$ . The Fermi level is set to zero and is indicated by the dashed lines.

$n_i$ : Number of atom

$\mu_O$ : chemical potentials of O atom

$\mu_{Se}$ : chemical potentials of Se atom

DOL: dimethoxyethane solvent for Na-S electrolyte

DME: 1,3-dioxolane solvent for Na-S electrolyte

PDOS: Partial density-of-state

$E_{gap}$ : Semiconductor band gap

Ti: Titanium

C: Carbon

O: Oxygen

Pham Vu Nhat, Duy Khanh Nguyen: Supervision, Reviewing and Editing the manuscript.

Minh Triet Dang: Conceptualization, Supervision, Funding acquisition, Writing- Original draft preparation, Reviewing and Editing the manuscript.

## ACKNOWLEDGEMENTS

This research is partly funded by the Ministry of Education and Training, Vietnam (Grant number B2024-TCT-16) and Can Tho University (Code: TSV2024-111). The authors acknowledge the Information and Network Management Centre at Can Tho University for providing high-performance computing resources.

## REFERENCES

1. Tarascon JM, Armand M. Issues and challenges facing rechargeable lithium batteries. *Nature*. 2001;414(6861):359–367. Available from: <https://doi.org/10.1038/35104644>.
2. Zhang S, Yao Y, Yu Y. Frontiers for Room-Temperature Sodium-Sulfur Batteries. *ACS Energy Lett.* 2021;6(2):529–536. Available from: <https://doi.org/10.1021/acsenergylett.0c02488>.

## CONFLICTS OF INTEREST

There are no conflicts to declare.

## AUTHOR CONTRIBUTION

To Trong Mai: Investigation, Writing- Original draft preparation, Reviewing and Editing the manuscript.  
Nguyen Truong Long: Conceptualization, Methodology, Investigation, Data curation, Writing, Reviewing and Editing the manuscript.

Duong Trong Nhan, Nguyen Thi Bao Trang: Investigation, Data curation.

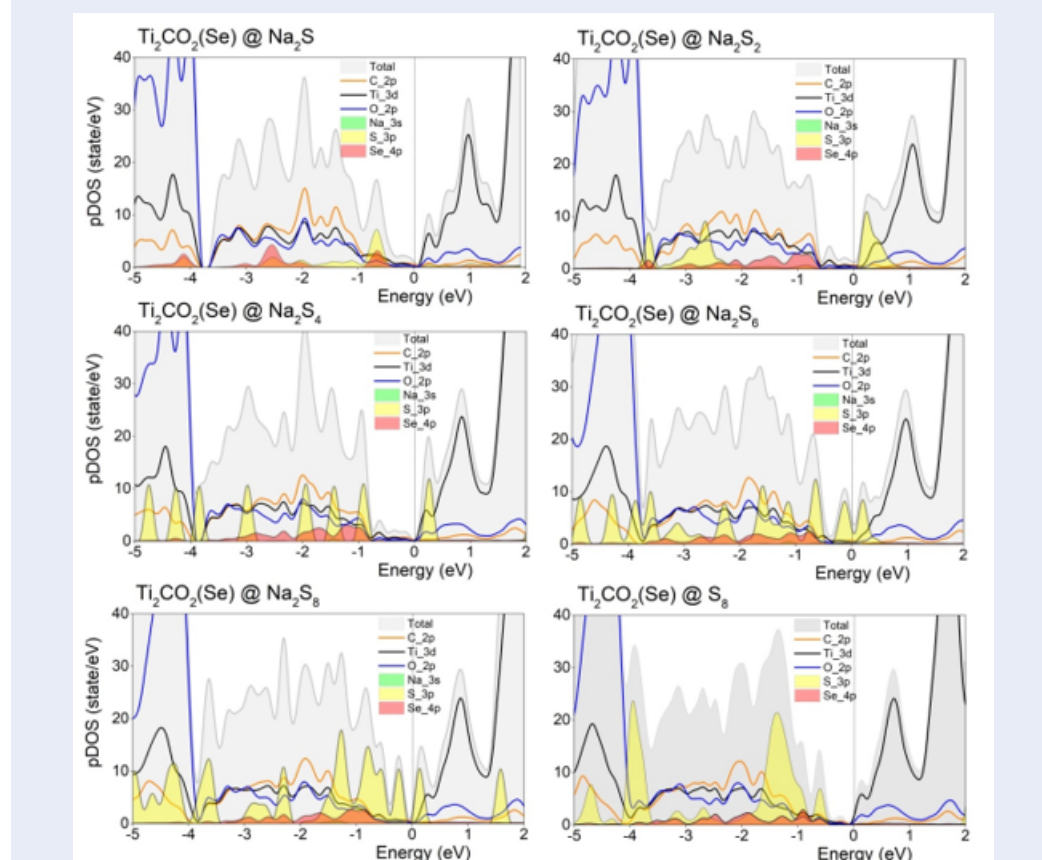


**Figure 6:** Projected density of states (PDOS) of  $\text{Na}_2\text{S}_x$  (where  $x = 1, 2, 4, 6, 8$ ) adsorbed on  $\text{Ti}_2\text{CO}_2(\text{Se})$ . The Fermi level is set to zero and is indicated by the dashed lines.

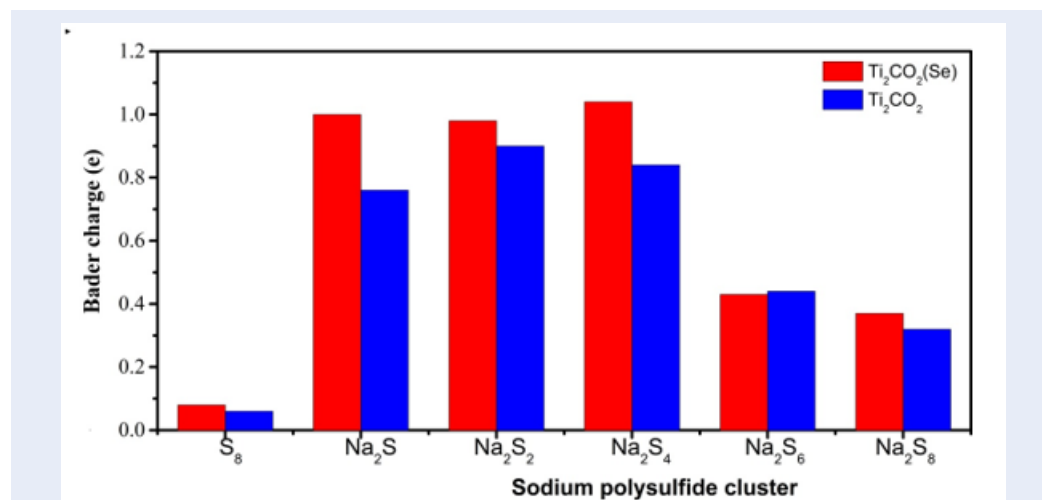


**Figure 7:** Bader charge transfers from  $\text{S}_8$  and  $\text{Na}_2\text{S}_x$  clusters adsorbed to 2D  $\text{Ti}_2\text{CO}_2(\text{Se})$  and bare 2D  $\text{Ti}_2\text{CO}_2$ . The amount of Bader charge is extracted as the difference between the Bader charge calculated for the clusters adsorbed on MXene and the bare  $\text{S}_8/\text{Na}_2\text{S}_x$  molecules.

3. Fang R, Zhao S, Sun Z, Wang DW, Cheng HM, Li F. More Reliable Lithium-Sulfur Batteries: Status, Solutions and Prospects. *Adv Mater.* 2017;29(48):1606823. Available from: <https://doi.org/10.1002/adma.201606823>.
4. Wang Y, Chen R, Chen T, Lv H, Zhu G, Ma L, et al. Emerging non-lithium ion batteries. *Energy Storage Mater.* 2016;4:103–129. Available from: <https://doi.org/10.1016/j.ensm.2016.04.001>.
5. Aslam MK, Niu Y, Na MX, Ca K, Mg, Al. Batteries and Super-capacitors. MXenes for Non-Lithium-Ion. 2021;11. Available from: <https://doi.org/10.1002/aenm.202000681>.
6. Liang X, Pang Q, Kochetkov IR, Sempere MS, Huang H, Sun X, et al. A facile surface chemistry route to a stabilized lithium metal anode. *Nat Energy.* 2017;2(9):17119. Available from: <https://doi.org/10.1038/nenergy.2017.119>.
7. Adelhelm P, Hartmann P, Bender CL, Busche M, Eufinger C, Janek J. From lithium to sodium: cell chemistry of room temperature sodium-air and sodium-sulfur batteries. *Beilstein J Nanotechnol.* 2015;6:1016–1055. Available from: <https://doi.org/10.3762/bjnano.6.105>.
8. Thatsam N, Tangpakonsab P, Moontragoon P, Umer R, Hussain T, Kaewmaraya T. Two-dimensional titanium carbide (Ti<sub>3</sub>C<sub>2</sub>T<sub>x</sub>) MXenes to inhibit the shuttle effect in sodium-sulfur batteries. *Phys Chem Chem Phys.* 2022;24(7):4187–4195. Available from: <https://doi.org/10.1039/D1CP05300K>.
9. Yu TT, Gao PF, Zhang Y, Zhang SL. Boron-phosphide monolayer as a potential anchoring material for lithium-sulfur batteries: A first-principles study. *Appl Surf Sci.* 2019;486:281–286. Available from: <https://doi.org/10.1016/j.apsusc.2019.05.019>.
10. Xiang P, Tian Z, Li Y, Gao Y, Wang Z, Chen L. Theoretical exploration of the structural evolution of sodium sulfide clusters in Na-S batteries. *Appl Surf Sci.* 2023;613:155906. Available from: <https://doi.org/10.1016/j.apsusc.2022.155906>.
11. Wang YX, Yang J, Lai W, Chou SL, Gu QF, Liu HK, et al. Achieving High-Performance Room-Temperature Sodium-Sulfur Batteries With S@Interconnected Mesoporous Carbon Hollow Nanospheres. *J Am Chem Soc.* 2016;138(51):16576–16579. Available from: <https://doi.org/10.1021/jacs.6b08685>.
12. Jayan R, Islam MM. Mechanistic Insights into Interactions of Polysulfides at VS2 Interfaces in Na-S Batteries: A DFT Study. *ACS Appl Mater Interfaces.* 2021;13(30):35848–35855. Available from: <https://doi.org/10.1021/acsmami.1c10868>.
13. Kaewmaraya T, Hussain T, Umer R, Hu Z, Zhao XS. Efficient Suppression of the Shuttle Effect in Na-S Batteries with an As<sub>2</sub>S<sub>3</sub> Anchoring Monolayer. *Phys Chem Chem Phys.* 2020;22:27300. Available from: <https://doi.org/10.1039/D0CP05507G>.
14. Bilibana M. Electrochemical properties of MXenes and applications. *Adv Sens Energy Mater.* 2023;2(4):100080. Available from: <https://doi.org/10.1016/j.asems.2023.100080>.
15. Patil SA, Marichev KO, Patil SA, Bugarin A. Advances in the synthesis and applications of 2D MXene-metal nanomaterials. *Surfaces and Interfaces.* 2023;38:102873. Available from: <https://doi.org/10.1016/j.surfin.2023.102873>.
16. Li J, Liu H, Shi X, Li X, Li W, Guan E, et al. MXene-based anode materials for high performance sodium-ion batteries. *J Colloid Interface Sci.* 2024;658:425–440. Available from: <https://doi.org/10.1016/j.jcis.2023.12.065>.
17. Zhang T, Zhang L, Hou Y. MXenes: Synthesis strategies and lithium-sulfur battery applications. *eScience.* 2022;2(2):164–182. Available from: <https://doi.org/10.1016/j.esci.2022.02.010>.
18. Chattopadhyay J, Pathak TS, Santos DMF. Applications of Polymer Electrolytes in Lithium-Ion Batteries: A Review. 2019;15.
19. Giannozzi P, Andreussi O, Brumme T, Bunau O, Nardelli MB, Calandra M, et al. Advanced capabilities for materials modelling with Quantum ESPRESSO. *J Phys Condens Matter.* 2017;29(46):465. Available from: <https://doi.org/10.1088/1361-648X/aa8f79>.
20. Perdew JP, Burke K, Ernzerhof M. Generalized gradient approximation made simple. *Phys Rev Lett.* 1996;77:3865. Available from: <https://doi.org/10.1103/PhysRevLett.77.3865>.
21. Prandini G, Marrazzo A, Castelli IE, Mounet N, Marzari; 2018. Available from: <http://materialscloud.org/sssp.https://doi.org/10.1038/s41524-018-0127-2>.
22. Lee K, Murray ED, Kong L, Lundqvist BI, Langreth DC. Higher-accuracy van der Waals density functional. *Phys Rev B.* 2010;82(8):81101. Available from: <https://doi.org/10.1103/PhysRevB.82.081101>.
23. Chakraborty D, Berland K, Thonhauser T. Next-generation nonlocal van der Waals density functional. *J Chem Theory Comput.* 2010;16(9):5893–5911. Available from: <https://doi.org/10.1021/acs.jctc.0c00471>.
24. Li N, Zhan Y, Wu H, Fan J, Jia J. Covalent surface modification of bifunctional two-dimensional metal carbide MXenes as sulfur hosts for sodium-sulfur batteries. *Nanoscale.* 2022;14(45):17027–17035. Available from: <https://doi.org/10.1039/D2NR03462J>.
25. Wang C, Han H, H, Guo Y. Stabilities and electronic properties of vacancy-doped Ti<sub>2</sub>CO<sub>2</sub>. *Comput Mater Sci.* 2019;159:127–135. Available from: <https://doi.org/10.1016/j.commatsci.2018.12.007>.
26. Tang W, Sanville E, Henkelman G. A grid-based bader analysis algorithm without lattice bias. *J Phys: Condens Matter.* 2009;21(8):84204. Available from: <http://dx.doi.org/10.1088/0953-8984/21/8/084204>.
27. Otero-De-La-Roza A, Johnson ER, Luană V. Critic2: A program for real-space analysis of quantum chemical interactions in solids. *Comput Phys Commun.* 2014;185(3):1007–1018. Available from: <https://doi.org/10.1016/j.cpc.2013.10.026>.
28. Faraji M, Bafekey A, Fadlallah MM, Molaei F, Hieu NN, Qian P, et al. Surface modification of titanium carbide MXene monolayers (Ti<sub>2</sub>C and Ti<sub>3</sub>C<sub>2</sub>) via chalcogenide and halogenide atoms. *Phys Chem C.* 2021;23(28):15319–15328. Available from: <https://doi.org/10.1039/D0CP05507G>.
29. Zhang Y, Zha XH, Luo K, Qiu N, Zhou Y, He J, et al. Tuning the electrical conductivity of Ti<sub>2</sub>CO<sub>2</sub> MXene by varying the layer thickness and applying strains. *Zhang J Phys Chem C.* 2019;123(11):6802–6811. Available from: <https://doi.org/10.1021/acs.jpcc.8b10888>.
30. Komen P, Ngamwongwan L, Junghawan S, Junkaew A, Suthirakun S. Promoting electrochemical performance of Ti<sub>3</sub>C<sub>2</sub>O<sub>2</sub> MXene-based electrodes of alkali-ion batteries via S doping: theoretical insight. *ACS Appl Mater Interfaces.* 2021;13(48):57306–57316. Available from: <https://doi.org/10.1021/acsmami.1c17802>.
31. Jayan R, Islam MM. Mechanistic insights into interactions of polysulfides at VS2 interfaces in Na-S batteries: a DFT study. *ACS Appl Mater Interface.* 2021;13(30):35848–35855. Available from: <https://doi.org/10.1021/acs.jpcc.1c00467>.
32. Nahian MS, Jayan R, Kaewmaraya T, Hussain T, Islam MM. Elucidating synergistic mechanisms of adsorption and electrocatalysis of polysulfides on double-transition metal MXenes for Na-S batteries. *ACS Appl Mater Interfaces.* 2023;14(8):10298–10307. Available from: <https://doi.org/10.1021/acsmami.1c22511>.
33. Li XH, Li SS, Cui XH, Zhang RZ, Cui HL. First-principle study of electronic properties and quantum capacitance of lithium adsorption on pristine and vacancy-defected O-functionalized Ti<sub>2</sub>C MXene. *Appl Surf Sci.* 2021;563:1502. Available from: <https://doi.org/10.1016/j.apsusc.2021.150264>.
34. He Q, Yu B, Li Z, Zhao Y. Density functional theory for battery materials. *Energy Environ Mater.* 2019;2(4):264–279. Available from: <https://doi.org/10.1002/eem2.12056>.
35. Zhou Q, Wang L, Ju W, Zhao Z, Hou J, Yong Y, et al. Effect of doping on the sensitivity of Ti<sub>2</sub>CO<sub>2</sub> toward NO: A DFT study. *Phys Lett A.* 2023;477:128919. Available from: <https://doi.org/10.1016/j.physleta.2023.128919>.
36. Gao X, Zhou Y, Tan Y, Cheng Z, Yang B, Ma Y, et al. Exploring adsorption behavior and oxidation mechanism of mercury on monolayer Ti<sub>2</sub>CO<sub>2</sub> (MXenes) from first principles. *Appl Surf Sci.* 2019;464:53–60. Available from: <https://doi.org/10.1016/j.apsusc.2018.09.071>.

37. Dang MT, Long NT, Phung VBT, Trang NTB, Nguyen TA, Tran TN, et al. Resolving adsorption mechanism of sodium polysulfides on  $Ti_{1-x}C_{x}M_xO_2$  MXenes for application in sodium-sulfur batteries: a first-principles study. *Appl Surf Sci.* 2024;.

# Nghiên cứu cơ chế hấp phụ của cụm sodium polysulfide trên bề mặt vật liệu MXene $\text{Ti}_2\text{CO}_2$ pha tạp selenium ứng dụng cho pin natri-sulfur

Tô Trọng Mãi<sup>1</sup>, Nguyễn Trường Long<sup>1</sup>, Dương Trọng Nhân<sup>2,3</sup>, Nguyễn Thị Bảo Trang<sup>1,4</sup>, Phạm Vũ Nhật<sup>5</sup>,  
Nguyễn Duy Khanh<sup>2,3</sup>, Đặng Minh Triết<sup>1,\*</sup>



Use your smartphone to scan this QR code and download this article

<sup>1</sup>Khoa Sư phạm Vật lý, Đại học Cần Thơ, Đường 3/2, Cần Thơ, Việt Nam

<sup>2</sup>Phòng thí nghiệm Vật lý tính toán, Viện Khoa học tính toán và Trí tuệ nhân tạo, Trường Đại học Văn Lang, Thành phố Hồ Chí Minh, Việt Nam

<sup>3</sup>Khoa Kỹ thuật Cơ – Điện và Máy tính, Trường Công nghệ, Trường Đại học Văn Lang, Thành phố Hồ Chí Minh, Việt Nam

<sup>4</sup>Đại học FPT, 600 Nguyễn Văn Cừ, Cần Thơ, Việt Nam

<sup>5</sup>Bộ môn Hóa, Đại học Cần Thơ, Đường 3/2, Cần Thơ, Việt Nam

## TÓM TẮT

Pin natri-sulfur (Na-S) ở nhiệt độ phòng là một giải pháp đầy tiềm năng của ngành lưu trữ năng lượng trong tương lai. Tuy nhiên, một số các thách thức về mặt kỹ thuật như hiệu ứng con thoi và độ dẫn điện kém đã làm cản trở ứng dụng thực tế của pin Na-S. Hiệu ứng con thoi (shuttle effect) không chỉ dẫn đến suy hao năng lượng mà còn làm giảm hiệu suất điện hóa của pin. Sự di chuyển của các polysulfide sẽ làm giảm dẫn dung lượng pin cũng như hiệu năng của chu trình nạp-xả. Ngoài ra, độ dẫn điện thấp có thể cản trở quá trình truyền điện tích, làm chậm quá trình động học phản ứng và làm giảm hiệu suất tổng thể của pin. Một cách tiếp cận hiệu quả để giải quyết những vấn đề này là sử dụng vật liệu hai chiều (2D) MXene làm vật liệu neo giữ (anchoring materials) điện cực, có thể giúp ngăn chặn hiệu ứng con thoi và tăng khả năng độ dẫn điện của pin natri-sulfur. Chúng tôi nghiên cứu tác động của việc pha tạp các nguyên tử selenide vào MXene dựa trên nguyên lý ban đầu để cải thiện độ ổn định và các tính chất điện tử của pin natri-sulfur. Các nguyên tử selenide được đưa vào lớp trung gian để giúp thu giữ các cụm natri-polysulfide. Kết quả của việc pha tạp các nguyên tử selenide, nhờ tương tác giữa các orbital Se-4p và S-3p đã làm tăng khả năng hấp phụ các cụm  $\text{Na}_2\text{S}$  và  $\text{Na}_2\text{S}_2$  so với vật liệu MXene trước pha tạp. Chúng tôi đã khảo sát chi tiết cơ chế liên kết giữa các cụm  $\text{Na}_2\text{S}_x$  và MXene pha tạp selenide. Kết quả cũng cho thấy sự khác biệt trong cơ chế hấp phụ giữa các cụm polysulfide có hàm lượng lưu huỳnh thấp ( $\text{Na}_2\text{S}$ ,  $\text{Na}_2\text{S}_2$  và  $\text{Na}_2\text{S}_4$ ) và các cụm có hàm lượng lưu huỳnh cao ( $\text{Na}_2\text{S}_6$  và  $\text{Na}_2\text{S}_8$ ), tập trung vào quá trình truyền điện tích và các tính chất điện tử. Cấu trúc đặc biệt của MXene cho phép chúng tương tác hiệu quả với polysulfide, giúp ngăn chặn hiệu ứng con thoi nhờ đó ngăn ngừa sự di chuyển của cụm polysulfide và giảm tổn thất năng lượng. Hơn nữa, nhờ sự kết hợp này, độ dẫn điện của hệ được cải thiện giúp tăng đáng kể hiệu suất tổng thể của pin natri-sulfur. Kết quả của chúng tôi nhấn mạnh khả năng của việc pha tạp selenide trong vật liệu điện cực hai chiều MXene để giúp tăng cường cơ chế hấp phụ natri polysulfide trong ứng dụng cho pin sạc natri-sulfur.

**Từ khóa:** Pin natri-sulfur, MXenes, pha tạp Selenium, vật liệu neo giữ (anchoring materials), lý thuyết phiếm hàm mật độ

## Liên hệ

Đặng Minh Triết, Khoa Sư phạm Vật lý, Đại học Cần Thơ, Đường 3/2, Cần Thơ, Việt Nam

Email: dmtriet@ctu.edu.vn

## Lịch sử

- Ngày nhận: 04-11-2024
- Ngày sửa đổi: 25-12-2024
- Ngày chấp nhận: 10-10-2025
- Ngày đăng: xx-xx-2026

## DOI:



## Bản quyền

© ĐHQG Tp.HCM. Đây là bài báo công bố mở được phát hành theo các điều khoản của the Creative Commons Attribution 4.0 International license.



**Trích dẫn bài báo này:** Trọng Mãi T, Trường Long N, Trọng Nhân D, Bảo Trang N T, Vũ Nhật P, Duy Khanh N, Minh Triết D. **Nghiên cứu cơ chế hấp phụ của cụm sodium polysulfide trên bề mặt vật liệu MXene  $\text{Ti}_2\text{CO}_2$  pha tạp selenium ứng dụng cho pin natri-sulfur.** *Sci. Tech. Dev. J. - Eng. Tech.* 2026; x(x):xxxx-xxxx.